Petroleum Science 21 (2024) 2734–2744

Contents lists available at ScienceDirect

Petroleum Science

journal homepage: www.keaipublishing.com/en/journals/petroleum-science

Original Paper

Securing offshore resources development: A mathematical investigation into gas leakage in long-distance flexible pipes

Xiang-An Lu [a], Liang-Liang Jiang [b, *], Jian-Sheng Zhang [c], Min-Gui Wang [a]

[a] Guangling College of Yangzhou University, Yangzhou, 225131, Jiangsu, China
[b] Department of Chemical and Petroleum Engineering, University of Calgary, Calgary, T2N 1N4, Alberta, Canada
[c] Department of Energy and Power Engineering, Tsinghua University, Beijing, 100084, China

ARTICLE INFO

Article history:
Received 18 August 2023
Received in revised form
22 December 2023
Accepted 23 January 2024
Available online 1 February 2024

Edited by Jie Hao and Meng-Jiao Zhou

Keywords:
Offshore resources development
Transport security
Long-distance flexible pipes
Gas leakage
Heat and mass transfer model
Finite difference calculation

ABSTRACT

Gas flexible pipes are critical multi-layered equipment for offshore oil and gas development. Under high pressure conditions, small molecular components of natural gas dissolve into the polymer inner liner of the flexible pipes and further diffuse into the annular space, incurring annular pressure build-up and/or production of acidic environment, which poses serious challenges to the structure and integrity of the flexible pipes. Gas permeation in pipes is a complex phenomenon governed by various factors such as internal pressure and temperature, annular structure, external temperature. In a long-distance gas flexible pipe, moreover, gas permeation exhibits non-uniform features, and the gas permeated into the annular space flows along the metal gap. To assess the complex gas transport behavior in long-distance gas flexible pipes, a mathematical model is established in this paper considering the multiphase flow phenomena inside the flexible pipes, the diffusion of gas in the inner liner, and the gas seepage in the annular space under varying permeable properties of the annulus. In addition, the effect of a variable temperature is accounted. A numerical calculation method is accordingly constructed to solve the coupling mathematical equations. The annular permeability was shown to significantly influence the distribution of annular pressure. As permeability increases, the annular pressure tends to become more uniform, and the annular pressure at the wellhead rises more rapidly. After annular pressure relief followed by shut-in, the pressure increase follows a convex function. By simulating the pressure recovery pattern after pressure relief and comparing it with test results, we deduce that the annular permeability lies between 123 and 512 mD. The results help shed light upon assessing the annular pressure in long distance gas flexible pipes and thus ensure the security of gas transport in the emerging development of offshore resources.

1. Introduction

The development of offshore natural gas resources necessitates substantial subsea natural gas to be transported to platforms or collection vessels through flexible pipes (Provasi et al., 2022), which possess the advantage of being non-fixed pipelines and are widely used for offshore natural gas transportation (Ren et al., 2020). The offshore gas flexible pipes feature a multi-layered structure (Liu et al., 2020), as shown in Fig. 1. In general, using polyethylene (PE) or polyvinyl chloride (PVC), the inner sheath is completely sealed. To improve the mechanical strength of the flexible pipes, the pressure sealing layer is wrapped with a compression-resistant layer and a tensile-resistant layer, which together form the annular space of the flexible pipes (Vantadori et al., 2019). As it shows in Fig. 1, the compression-resistant layer and the tensile-resistant layer are not completely sealed, yielding gaps. The outermost layer is a protective layer, which is usually made of high polymer material (Li et al., 2020). However, in unfavorable conditions it is likely for the polymer material to progressively degrade and dissolve, allowing gas molecules to diffuse inside. Under high gas pressure conditions in the bore, gas dissolves into inner liner layer and diffuses subsequently. Consequently, gas aggregates in the metal structure gaps causing annular pressure to rise. Reports show that changes in the annual condition may

* Corresponding author.
E-mail address: jial@ucalgary.ca (L.-L. Jiang).

https://doi.org/10.1016/j.petsci.2024.01.020

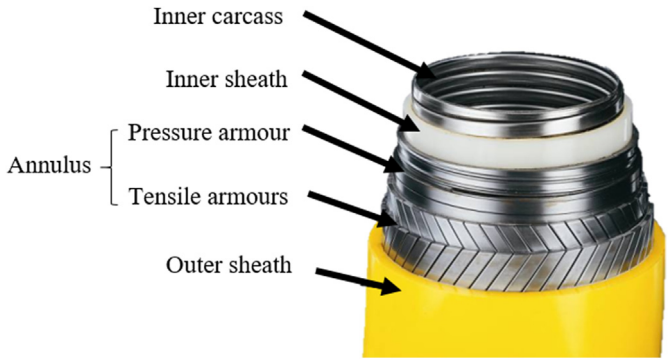

Fig. 1. Flexible pipes structure.

adversely affect the integrity of the flexible pipes. For example, a bulge or even rupture may occur in the flexible pipes' outer sheath layer due to an excessive annular pressure (Chen et al., 2021). It is thus a common practice to release the annual pressure to protect flexible pipes. In addition, the presence of acid gases like H_2S and CO_2 results in an acidic environment in the annular space. This acidic environment promotes a corrosion of the metal structure, posing a notable challenge to the mechanical structure of flexible pipes. Furthermore, gas dissolved in the high polymer layer will subsequently impair the mechanical properties of the material (Emileh et al., 2007).

The permeation behavior of gases in polymer materials has been extensively studied in the literature. It is suggested that the coiled shape of polymer molecules provides space for the diffusion of small molecules. Under pressure effects gas molecules dissolve into polymer materials (Scheichl et al., 2005). The dissolution and diffusion of gas molecules within the polymer material are dependent on many factors, e.g., external pressure, temperature, the molecular structure, and the crystallinity of the polymer material (Sadrzadeh et al., 2011). Specifically, the ability of gas molecules to dissolve in polymer materials is generally described by the solubility coefficient, while the ability of gas molecules to migrate within polymer materials is described by the diffusion coefficient. An Arrhenius-type equation can be used to describe the effect of temperature on the solubility and diffusion coefficients (Flaconneche et al., 2001).

The diffusion of gas molecules in polymer materials follows Fick's first law (Li and Long, 1969). Combining the conservation equation of mass, the mass transfer equation of gas molecules in polymer materials can be deduced. For one-dimensional equations, an analytical solution is obtainable by combining initial and boundary conditions (Rutherford and Do, 1997). Difference or finite element methods can be used for numerical solutions to problems with complex boundary conditions, permitting a suitable description of the gas permeation behavior in tubular polymer materials. The computational methods to predict gas permeation behavior can be referred to elsewhere (Ash, 2001).

Transmitting fluid in the offshore long-distance gas flexible pipes is generally a multiphase transport problem in a high temperature, high pressure environment. In addition, the gas permeability in the pipe appears heterogeneous along the flexible pipes. Wang et al. (2021) performed numerical simulation on gas permeation in flexible pipes, taking into account the impact of changes in the fluid flow state within the flexible pipes. It was shown that a change in the fluid flow state will result in variations in pressure and temperature along the length of the flexible pipes. Furthermore, the structure and conditions in the annular space of the flexible pipes would further alter gas permeation (Wang et al., 2009). Fig. 2 is a schematic diagram of gas permeation behavior in the transmission flexible pipes, which illustrates that under favorable conditions gas within the flexible pipes permeates through the inner liner and enters the annular space. Due to the annular structure of the flexible pipes, the metal compression layer and the adhesion of the polymer material in the annulus exert a shielding effect on gas permeation.

In long gas transmission flexible pipes, gas in the annular space flows through the metal gaps within the annular space, and macroscopically forms bulk flow along the length of the flexible pipes. This article aims to shed light upon the complex gas flow behavior in the long-distance gas flexible pipes. Encompassing the abovementioned multiple gas transport mechanisms involved, namely the multiphase flow inside the flexible pipes, the diffusion of gas in the inner liner, and the gas seepage in the annular space, a mathematical model is developed to describe the gas permeation in the flexible pipes considering the effect of temperature, and the numerical method for solving the mathematical equations is established. The calculated results would lay a theoretical foundation for the prediction of changes in annular space pressure in long flexible pipes. It is to note that the lack of relevant data and research in this topic makes it an impossible task to validate the model at this stage. It is thus the hope that the investigation in this paper serves to galvanize future studies from scholars and engineers.

2. Mathematical model

2.1. Gas flow in pipe

In offshore gas fields development, product gas is transported to platforms via flexible pipes. Typically, gas wells produce water during the extraction process, resulting in multiphase flow in the gas pipeline. Multiphase flow in pipelines is a crucial and prevailing phenomenon in oil and gas production, and therefore there is a wealth of research in this area. To predict the liquid holdup and pressure gradient in various flow patterns, a few mechanistic models have been developed for vertical flow (Shoham, 2006; Ansari et al., 1994; Al-Safran and Brill, 2017). For instance, in the two-phase vertical flow in pipes, the common flow patterns include annular flow, slug flow, bubble flow, and dispersed bubble flow (Wu et al., 2017). Taitel et al. (1980) established a widespread model

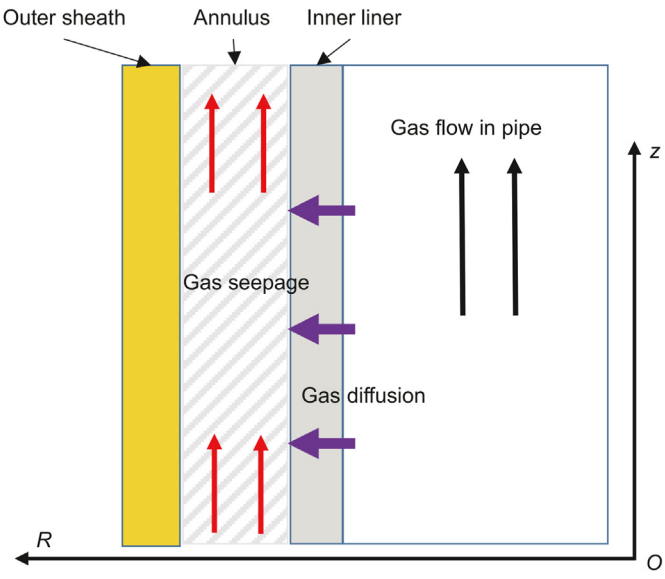

Fig. 2. Schematic diagram of gas permeation behavior in flexible pipes.

to predict flow pattern, which was further modified to consider the effect of the inclination angle on the upward flow behavior (Barnea et al., 1985).

Many suitable models of fluid flow have been adopted in commercial simulators, which generally yield accurate calculations of pressure and temperature changes along the pipeline under complex operating conditions. In this paper, the main focus is on the gas permeation in the flexible pipe, and thus the modelling results of gas flow in the pipeline are applied as the proper boundary conditions. The calculation of pressure and temperature distribution inside the pipe was performed using Pipesim software.

2.2. Gas diffusion in inner liner

2.2.1. Mass transfer model

The cross-sectional profile structure of the transmission flexible pipes is sketched in Fig. 3. The internal pressure of the flexible pipes is P_u; the inner and outer radii of the polymer internal pressure sealing layer are R_0 and R_1 respectively, whereas the bounding radii of the polymer protective layer are R_2 and R_3 as it shows in Fig. 3.

The space between the polymer internal pressure sealing layer and the outer protective layer composes the annulus layer. The metal compressive and tensile layers in the annulus are not completely closed, and their gaps can be represented by the porosity φ, and the volume of the side annulus can be calculated by the following formula:

$$V_a = \pi\left(R_2^2 - R_1^2\right)\varphi L \tag{1}$$

where L is the length of the flexible pipes. The mass transfer process of gas in each layer satisfies Fick's law. In the radial coordinate system, the diffusion equation of gaseous component is shown in Eq. (2):

$$\frac{\partial C_{i,k}}{\partial t} = \frac{1}{r}\frac{\partial}{\partial r}\left(rD_{i,k}(T)\frac{\partial C_{i,k}}{\partial r}\right) + \frac{\partial}{\partial z}\left(D_{i,k}(T)\frac{\partial C_{i,k}}{\partial z}\right) \tag{2}$$

where, $C_{i,k}$ and $D_{i,k}$ represent the concentration and diffusion coefficient of gas component i in the layer k, respectively; z is the extension direction of the flexible pipes. The diffusion coefficient is a function of temperature, which is reasonably described with an Arrhenius equation as follows (Sadrzadeh et al., 2011):

$$D_{i,k} = D_{i0}\exp\left(-\frac{E_{i,k}}{8.314\times(273.15+T)}\right) \tag{3}$$

where $E_{i,k}$ is the activation energy of gas component i in the k layer.

(2) Initial boundary condition

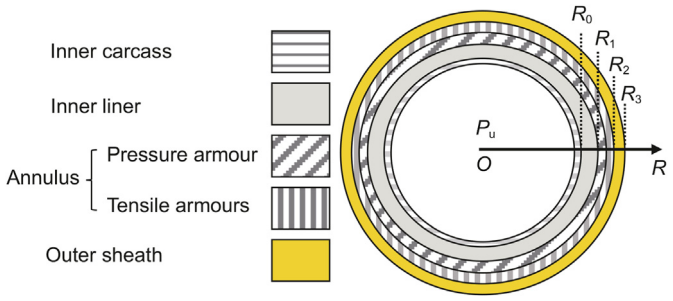

Fig. 3. Schematic diagram of flexible pipes' cross-sectional structure.

Due to a high pressure inside the pipeline, the gas molecules gradually dissolve into the adjacent internal pressure sealing layer and diffuse subsequently in it. The concentration of dissolved gas is calculated by Eq. (4) (Wang et al., 2021):

$$C_{i,r0} = \frac{P_u S_i(T)}{V_n} \tag{4}$$

In which $C_{i,r0}$ is the concentration of the gas component i that can dissolve into the polymer material under the condition of pressure P_u and temperature T; V_n is the gas volume constant and equals 2.24×10^{-4} m^3/mol; S_i is the temperature-dependent solubility which takes the following form (Wang et al., 2021):

$$S_i = S_{i0}\exp\left(-\frac{H_i}{8.314\times(273.15+T)}\right) \tag{5}$$

where S_{i0} is the solubility coefficient and H_i is the apparent heat of solution. The inner radius of the polymer material internal pressure closed layer is R_0, thus the inner boundary conditions of the diffusion equation at R_0 can be expressed by Eq. (6):

$$C(R_0,t) = \min\left(C_{i,R_0}, C_{i,u}\right) \tag{6}$$

where $C_{i,u}$ is the concentration of gas component i in the pipeline. The gas enters the annulus through diffusion, and at R_1, the outer boundary condition of the diffusion equation, the transport of gas is affected by the annulus condition. Generally, the annular conditions exert dual effects on the diffusion of gas. First, the metal compressive layer and the tensile layer of the annulus have a pressure effect on the polymer internal pressure sealing layer, which forms a shielding effect and impedes gas diffusion to the annulus. Second, the accumulation of gas diffused into the annulus leads to a rise in annular pressure, and the concentration of gas components in the annulus affects the diffusion of gas molecules from the inner pressure seal to the annulus. Based on the above two considerations, the third type of boundary conditions characterize the outer boundary conditions under the influence of annulus (Lu et al., 2023).

$$-D_i(T)\frac{\partial C_i}{\partial r} = h\left[C_i(R_1,t) - C_{i,a}(t)\right] \tag{7}$$

where $C_{i,a}$ is the concentration of annulus gas component i, and h is the shielding coefficient. When $h \gg D_i$, it indicates that gas molecules in the internal pressure sealing layer are bound to diffuse into the annulus layer, and the boundary conditions are reduced to the first type boundary conditions:

$$C_i(R_1,t) = C_{i,a}(t) \tag{8}$$

Under this condition, if the annulus is closed, the concentration of gas components in the annulus will continue to rise until an equilibrium state occurs. When $h \ll D_i$, which means that the gas molecules in the internal pressure sealing layer hardly diffuse into the annulus layer due to the shielding effect of the metal compressive and tensile layers on the gas diffusion. In this case, the boundary conditions degenerate to the second type boundary conditions:

$$-D_i(T)\frac{\partial C_i}{\partial r} \approx 0 \tag{9}$$

Under this condition, the shielding effect is nearly in full swing, and no gas penetrates the annulus. Apparently, this is an extreme under ideal circumstances. Practical cases fall between the two extremes, so it is more suitable to use the third type boundary

conditions to represent the influence of annular conditions.

The initial conditions can be expressed as the following equation:

$$C_i(r,0)=f(r) \tag{10}$$

The gas concentration distribution in the polymer internal pressure closed layer under the initial conditions plays a role in the calculation results. When the experiment uses a new tube or a tube that has been sitting for a long time, the initial conditions simplify to

$$C_i(r,0)=0 \tag{11}$$

Combining the diffusion equation, boundary conditions and initial conditions equations, a numerical solution is obtainable.

2.2.2. Heat transfer model

It can be seen from the diffusion coefficient equation and solubility equation that the temperature is a variable on the diffusion of gas. In addition, the pressure in the annulus is a function of temperature. Inside the offshore flexible pipes is the high temperature and high pressure fluid extracted from the gas reservoir. Therefore, heat is slated to transfer from the pipe to the external environment such as seawater, and a temperature gradient happens on the flexible pipes profile. In this physical process, the heat transfer equation in the layer k can be approximated by the following formula:

$$\rho_k c_k \frac{\partial T}{\partial t}=\frac{1}{r}\frac{\partial}{\partial r}\left(\lambda_k \frac{\partial T}{\partial r}\right)+\frac{\partial}{\partial z}\left(\lambda_k \frac{\partial T}{\partial z}\right) \tag{12}$$

where T is the temperature, ρ_k, c_k, and λ_k are the density, specific heat, and heat transfer coefficient of the layer k, respectively. Assuming a strong heat exchange capacity of various media, the boundary conditions take the form the first type:

$$T(R_0,t)=T_u \tag{13}$$

$$T(R_3,t)=T_s \tag{14}$$

where T_u is the fluid temperature inside the pipe, whereas T_s denotes the ambient sea water temperature surrounding the pipe.

Under general working conditions, the temperature inside the pipeline and in the external environment is largely an invariant. Compared with the mass transfer process, the heat transfer process is fast to establish a temperature equilibrium state. Therefore, it is a reasonable simplification to use the steady-state calculation results to characterize the influence of temperature on diffusion.

2.3. Gas seepage in annulus

Subsea pipelines connect offshore platforms to the seabed, typically spanning thousands of kilometers. In general, the internal gas pressure within the pipeline varies with the flow regime, gas-liquid ratio, and velocity. Due to the pressure heterogeneity within the pipeline, gas permeation rates vary at different nodes, resulting in variations in the direction of gas flow into the annulus. At the seabed, due to the effects of gravity and flow resistance, the pressure within the pipeline is relatively high, enabling gas permeation into the annulus to prevail. Treating the annulus as a porous medium, as shown in Fig. 4, the gas that permeated into the annulus through diffusion can flow along the length of the pipeline.

For a mathematical description, the pipeline can be discretized along its length, and the gas permeation process in the annulus can be described as a one-dimensional seepage process. Treating the gas in the annulus as a single-phase and neglecting the effect of gravity, the movement of the gas follows Darcy's law:

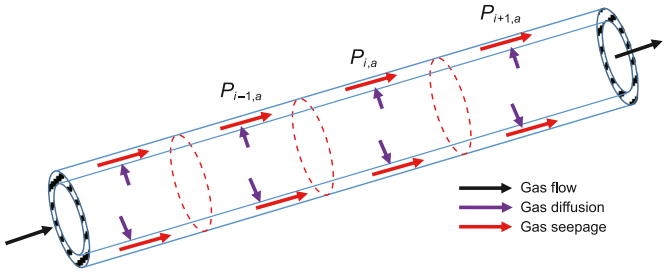

Fig. 4. Schematic diagram of gas flow and permeation direction in a long flexible pipe.

$$v=-\frac{K_g}{\mu}\frac{\partial p_a}{\partial x} \tag{15}$$

where K_g is the gas permeability of the annular space, μ is the gas phase viscosity, and p_a is the pressure in the annular space. According to the conservation equation of mass, the gas continuity equation can be obtained:

$$\frac{dm_g}{dVdt}-\frac{\partial \rho_g v}{\partial x}=\frac{\partial(\varphi\rho_g)}{\partial t} \tag{16}$$

where m_g is the mass of gas penetrating into the annulus, ρ_g is the density of the gas. Due to the compressibility of the gas, the relationship between the gas density, temperature and pressure can be expressed by the equation of state:

$$\rho_g=\frac{p_a M}{RT_a} \tag{17}$$

where R is the gas constant, T_a is the annular temperature, and M is the relative molecular mass of the gas. Substituting the equation of state and equation of motion into the continuity equation yields the pressure equation in the annulus:

$$\frac{\mu}{K_g}\frac{RT}{p_a M}\frac{dm_g}{dVdt}+\frac{\partial^2 p_a}{\partial x^2}=\frac{\mu\varphi}{K_g p_a}\frac{\partial p_a}{\partial t} \tag{18}$$

The pressure equation describes the process wherein gas diffuses into the annulus and subsequently establishes pressure equilibrium throughout the annulus. It can also describe the process of pressure propagation during annular gas discharge.

3. Calculation method

The forward difference method is used to discretize the diffusion equation and the heat transfer equation. Because the two equations have the same form, the difference equation is similar. The discrete form of the diffusion equation is expressed as follows:

$$C_j^{n+1}=aC_{j+1}^n+bC_j^n+cC_{j-1}^n \tag{19}$$

In the equation:

$$a=\frac{\Delta t}{\Delta r^2}\frac{r_{j+1}D_{j+1}}{r_j}+\frac{\Delta t}{\Delta z^2}D_{j+1} \tag{20}$$

$$b = 1 - \frac{\Delta t}{\Delta r^2}\frac{r_{j+1}D_{j+1} + r_j D_j}{r_j} - \frac{\Delta t}{\Delta z^2}2D_j \tag{21}$$

$$c = \left(\frac{\Delta t}{\Delta r^2} + \frac{\Delta t}{\Delta z^2}\right)D_j \tag{22}$$

The calculation stability condition of the forward difference equation is

$$\frac{\Delta t}{\Delta r^2}D \le 0.5, \frac{\Delta t}{\Delta z^2}D \le 0.5 \tag{23}$$

Combining the discrete forms of the boundary condition Eqs. (6)–(8), the complete discrete form of the diffusion equation is obtained.

The discrete form of the annular pressure propagation Eq. (18) along the pipe length can be described:

$$\frac{RT}{\varphi M}\frac{\mathrm{d}m_g}{\mathrm{d}V} + \frac{\Delta t}{\Delta x^2}\frac{K_g}{\mu\varphi}p^n_{a,i}\left(p^n_{a,i+1} + p^n_{a,i-1} - 2p^n_{a,i} + 1\right) = p^{n+1}_{a,i} \tag{24}$$

In the discrete Eq. (24), the left-hand side of the equation represents the pressure of gas diffusing from the inner liner into the annulus, and the pressure of gas permeating in the annulus.

The equations are solved numerically using Python, and the calculation process is shown in Fig. 5. As it shows, the program executes three nested loops: the innermost loop calculates the diffusion equation radially, the middle loop accounts for the gas seepage process along the annulus, and the outermost loop implements the influence of duration. Inside the pipeline, the multiphase flow information is considered as a boundary condition, whilst the pressure and temperature are the boundary conditions for the diffusion equation.

Fig. 6 gives the grid discretization method, wherein the inner liner is divided into grids along the radial direction. The gas permeation behavior and temperature field distribution in the polymer lining are calculated by solving the radial diffusion equation. The annulus is meshed along the direction of the flexible pipes, and the pressure propagation Eq. (24) is computed in a 1D mesh.

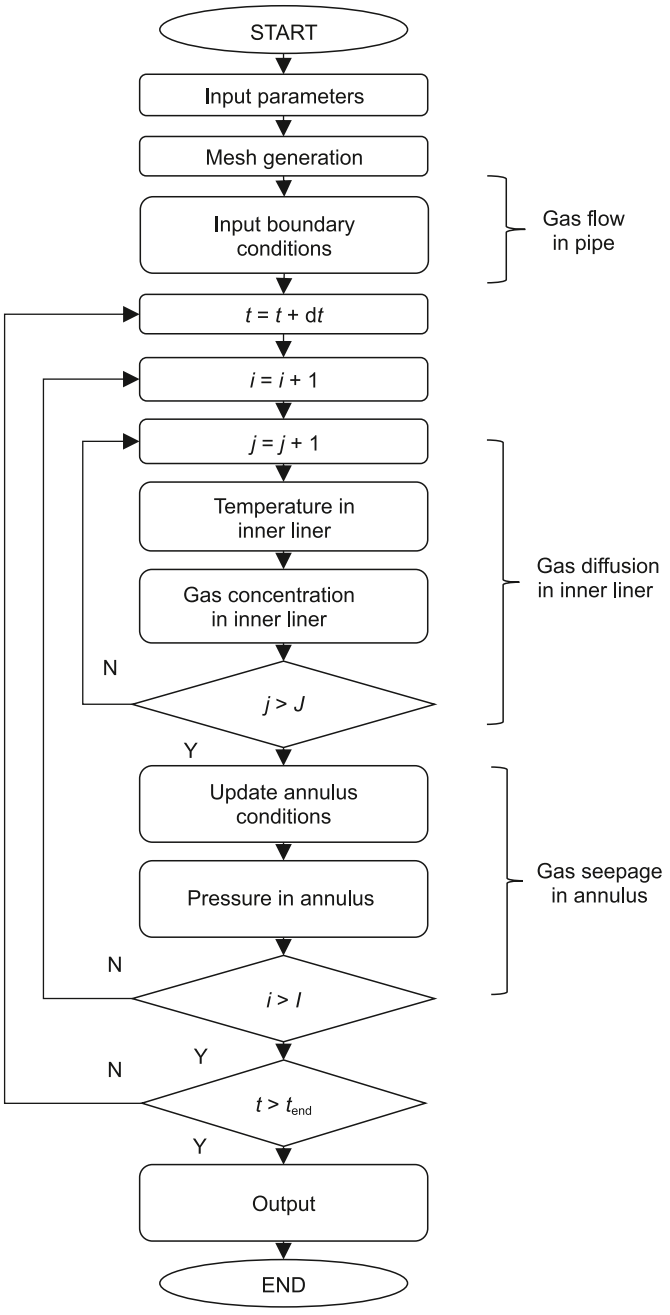

Fig. 5. Flowchart of calculation procedure.

4. Results and discussion

4.1. Gas flow in pipe

For the well of interest, viz Well A, Fig. 7 gives the measured data pertaining to the vertical depth and ambient seawater temperature of the gas flexible pipes. It illustrates that the 1056-m-long flexible pipes feature a zigzag shape in the sea. The seabed sits 545 m deep in the water and has a water temperature of 9.4 °C.

In the offshore development, the pressure and temperature of a gas reservoir gauge the fluid pressure and temperature in the gas production wellbore and pipeline. In the transport process, the pressure potential energy in the gas pipeline transforms into gravitational potential energy and energy loss. The fluid pressure and temperature in the gas pipeline of Well A along the pipeline length were modelled in a commercial simulator which are shown in Fig. 8, wherein the pressure varies with the length and depth of the pipeline. The pipeline has an initial internal pressure of 3.25 MPa and a temperature of 61.29 °C in the submarine section.

As fluid flows in the pipeline, the flow regime changes. For example, Table 1 lists the flow characteristics parameters of three calculation nodes at 300, 800, and 1000 m along the pipeline (also marked in Fig. 8). With an increase in gas velocity and a decrease in liquid holdup the flow regime changes from slug flow to annular flow.

4.2. Gas diffusion in inner liner

The relevant dimensions of the gas flexible pipes and the heat transfer parameters of each layer are shown in Table 2. The inner and outer diameters of the flexible pipes are 306 and 466 mm, respectively. The high density polyethylene (HDPE) composes the 11 mm-thick polymer lining material. The annulus forms a gas storage space, with a 0.02 m^3 annulus volume per unit length which yields an equivalent porosity of 0.26 for the annulus. With the aid of a total composition analyzer, Table 3 presents the composition test results of the sampled gas in the pipeline and the annulus. It demonstrates that the gas that penetrated into the

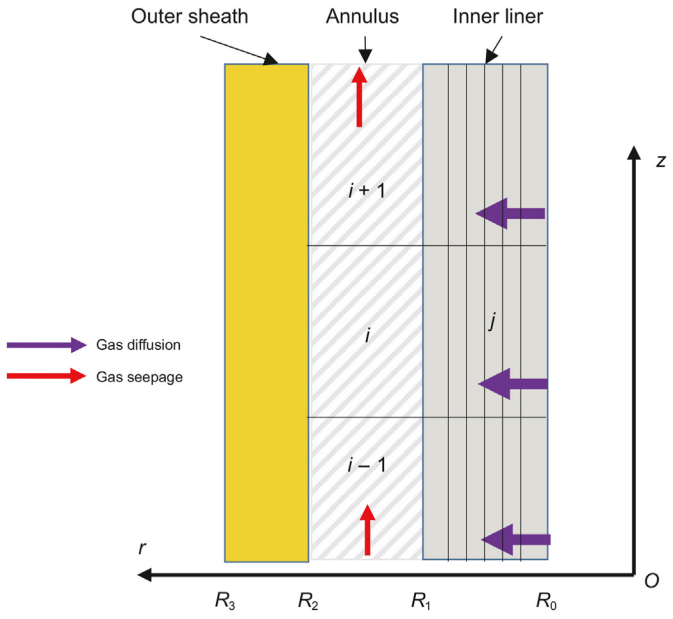

Fig. 6. Geometric discretization diagram.

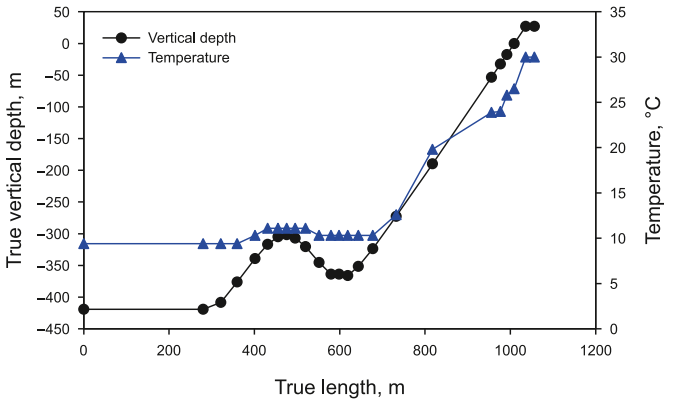

Fig. 7. Flexible pipes geometry and sea water temperature.

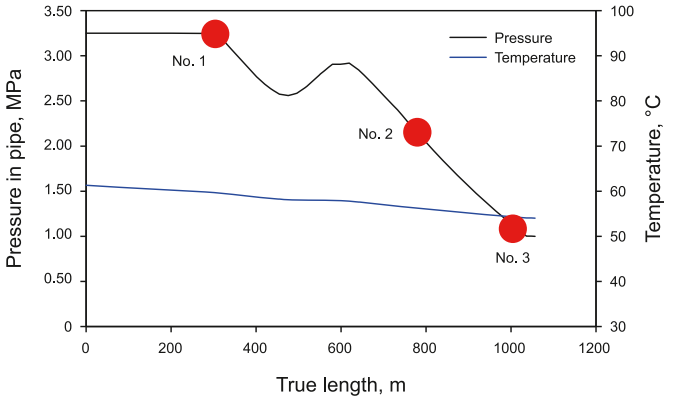

Fig. 8. Profile of pressure and temperature along the flexible pipes.

annulus through the polymer lining encompasses mainly CO_2, N_2, CH_4, and C_2H_6. The diffusion coefficients and solubility coefficients of these four gases in HDPE are taken values in the literature (Flaconneche et al., 2001; Merkel et al., 2000), as shown in Table 4.

To further reveal the diffusion behavior of gas in the polymer inner liner, the gas permeation results at the three nodes in Table 1 are calculated. The variance of temperature and pressure at the three nodes leads to differing solubility and diffusion ability of gas molecules in molecular materials. Fig. 9 shows the temperature distribution profiles of the three nodes. Node 1 is located at the actual length of 300 m, with a water depth of 402 m. It has an in-pipe temperature of 59.53 °C, and an ambient seawater temperature of 9.40 °C. Since the heat transfer capacity of the material is much lower than that of the annular metal layer, the temperature profile features a gradient in the polymer inner layer and the outer sheath layer, whereas a more even temperature distribution presents in the annulus as revealed in Fig. 9. In a quantitative presentation, the lowering temperature in the pipe (see Fig. 8) and increasing temperature in the seawater with pipe length attributed to a dwindling thermal gradient at the two sides of the annulus, as implied in the three nodes. For example, due to a big thermal gradient, at Node 1 the temperature falls from the highest of the three at the pipe core to the lowest near the annulus. As a result, the modelling shows that farthest Node 3 has a higher temperature profile in the annuls and the outer sheath than the other two nodes. The temperature in the annular space is mainly affected by the bounding temperatures at the two sides, namely the temperature of gas transporting in the pipe and the temperature of the sea water enclosing the pipe.

It is manifested in Fig. 9 that, at the No. 1 node, the computed annular space temperature is 27.48 °C, whereas it is 31.42 and 35.24 °C at the nodes of No. 2 and No. 3, respectively.

Along the length of the flexible pipes, the non-uniformity of gas pressure distribution and internal temperature of the flexible pipes lead to inconsistent diffusion behavior of the gas in the polymer liner at different points. Figs. 10–12 show the results of the total and gas component pressures in the annulus at the three nodes as a function of time. It is noteworthy that the pressures were computationally approximated with an assumption that the annulus at the node is in a closed state. The rate at which gas diffuses from the tube into the annulus depends on its ability to dissolve and diffuse in the polymer material. In general, the curves in Figs. 10–12 exhibit a similar trend that the pressure of gas component increases in a nearly quasi-linear fashion. Comparatively, gas gains the strongest diffusive capability at Node 1, with the annular pressure rising to 0.33 MPa in 30 d, while it is 0.23 and 0.12 MPa at Node 2 and Node 3, respectively. In a quantitative perspective, the modelling shows that gas diffusive capability at Node 1 is 2.75 times that of Node 3, indicating a notably varying gas diffusive capability along the flexible pipes.

Under actual conditions, the annulus is porous and the gas that penetrated the annulus will flow along the gaps in the metal layer. To evaluate the change in the annulus pressure along flexible pipes, it is thus necessary to consider the permeation behavior of the gas in the annulus.

4.3. Gas seepage in annulus

The behavior of gas permeation in the flexible pipes is mainly reflected by the pressure propagation of the gas phase. The gaps between the metal structure of the flexible pipes' annular tensile layer and compressive layer make it reasonable to consider mathematically the annular space as a porous medium, wherein the gas undergoes permeation under a pressure difference.

According to Darcy's law, the permeability of a medium is one of the main factors affecting gas permeation. For the annular space, the gas permeability depends on the structural characteristics of the annular space and the processing technology of the flexible pipes. Due to a lack of relevant data in this regard, a set of different

Table 1
Multiphase flow parameters at three nodes.

No.	True length, m	Pressure, MPa	Temperature, °C	Flow rate of gas, m/s	Flow pattern	Liquid holdup
1	300	3.18	59.53	0.82	Slug flow	0.86
2	800	2.04	56.02	1.52	Annular flow	0.71
3	1000	0.99	54.01	2.20	Annular flow	0.34

Table 2
The dimension parameters of gas flexible pipes.

	Parameter	Value	Unit
Geometric dimensions	Bore	306	mm
	Inner liner, HDPE	328	mm
	Annulus	454	mm
	Outer sheath	466	mm
	Void fraction of annulus	0.13	
Physical property	Density of inner liner	1650	kg/m^3
	Specific heat of inner liner	1.32	J/g·K
	Heat transfer coefficient of inner liner	0.14	J/m·K·s
	Density of metal in annulus	7620	kg/m^3
	Specific heat of metal in annulus	0.42	J/g·K
	Heat transfer coefficient of metal in Annulus	56.2	J/m·K·s
	Density of outer sheath	1030	kg/m^3
	Specific heat of outer sheath	2.1	J/g·K
	Heat transfer coefficient of outer sheath	0.28	J/m·K·s

Table 3
Molar concentration of components in inner pipe and annulus.

Component	Inner pipe, %	Annulus, %
CO_2	2.26	0.09
N_2	12.44	87.35
C_1	63.87	1.25
C_2	7.91	0.01
C_3	6.71	0.00
iC_4	1.91	0.00
nC_4	1.91	0.00
iC_5	0.68	0.00
nC_5	0.39	0.00
nC_6	0.76	0.00
nC_7	0.26	0.00
nC_8	0.09	0.00
nC_9	0.02	0.00
nC_{10}	0.01	0.00
C_{11+}	0.00	0.00
H_2O	0.78	0.00
O_2	0.00	11.30
Total	100	100

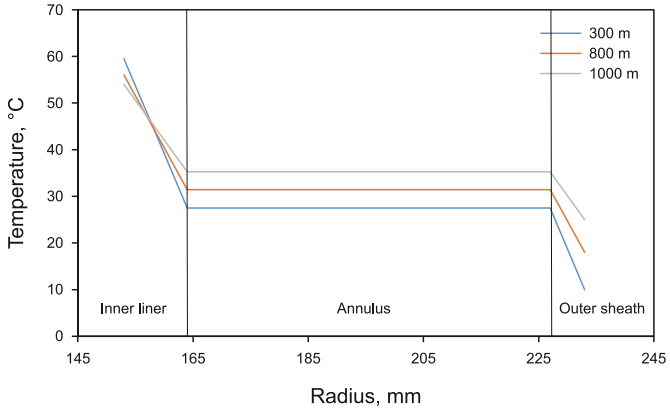

Fig. 9. Temperature profile at the selected three nodes.

annular gas permeability values were used to calculate the distribution of annular pressure along the length of the flexible pipes.

Fig. 13 shows the calculated results assuming an annular gas permeability of 0.1 mD. Under this tight condition, the gas that permeated into the annular space through the polymer inner liner barely flows along the flexible pipes. Since the pipes situate shallower as the length extends (see Fig. 7), it thus implies in Fig. 13 that the annular space at the deeper underwater position experiences a rapid pressure buildup. The pressure in the annular space is revealed to be unevenly distributed along the length, reflective of the in-pipe pressure distribution as shown in Fig. 8 due to a weak connection of gas in the annuls in a tight porous medium. At a higher annular gas permeability, e.g., 10 mD, Fig. 14 shows the

Table 4
Diffusion coefficient and solubility coefficient of gas components.

Component	Diffusion coefficient	Solubility coefficient	Reference
CO_2	$D = 2 \times 10^{-5} \exp\left(\frac{-43344}{8.314(T+273.15)}\right)$	$S = 2.71 \times 10^{-3} \exp\left(\frac{5353}{8.314(T+273.15)}\right)$	Flaconneche et al. (2001)
N_2	$D = 1.8 \times 10^{-5} \exp\left(\frac{-43321}{8.314(T+273.15)}\right)$	$S = 1.7 \times 10^{-7} \exp\left(\frac{4863}{8.314(T+273.15)}\right)$	Flaconneche et al. (2001)
C_1	$D = 3 \times 10^{-4} \exp\left(\frac{-43135}{8.314(T+273.15)}\right)$	$S = 1.7 \times 10^{-5} \exp\left(\frac{7885}{8.314(T+273.15)}\right)$	Flaconneche et al. (2001)
C_2	$D = 2.1 \times 10^{-4} \exp\left(\frac{-45841}{8.314(T+273.15)}\right)$	$S = 2 \times 10^{-6} \exp\left(\frac{6954}{8.314(T+273.15)}\right)$	Merkel et al. (2000)

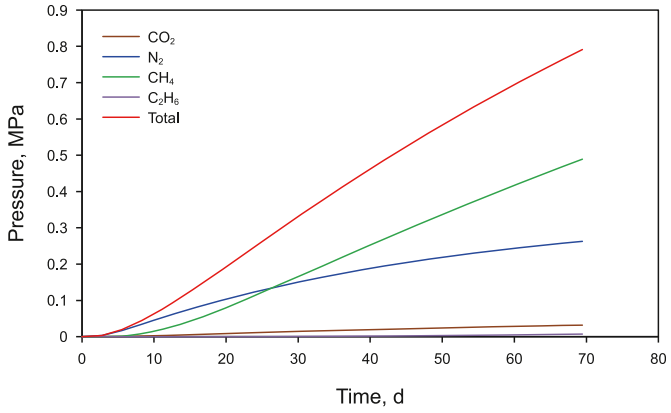

Fig. 10. Changes of gas pressure in the annulus with time at Node 1 (3.18 MPa, 59.53 °C in bore).

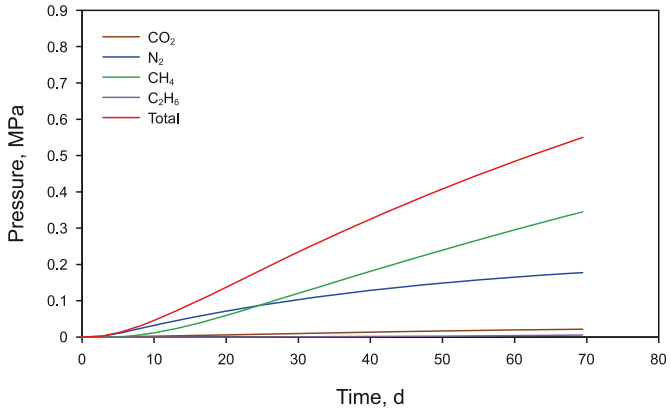

Fig. 11. Changes of gas pressure in the annulus with time at Node 2 (2.04 MPa, 56.02 °C in bore).

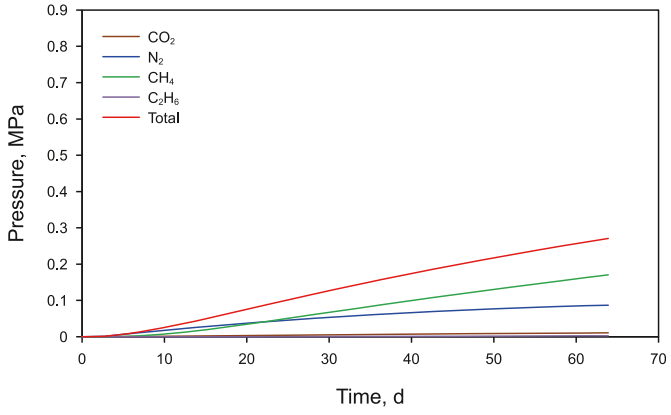

Fig. 12. Changes of gas pressure in the annulus with time at Node 3 (0.99 MPa, 54.01 °C in bore).

calculated results. Comparing with Fig. 13 yields that at a higher permeability value gas flow, resulting in a wider pressure spread-out. However, the pressure gradient along the pipe length suggests that the permeability in this situation is insufficient to free gas flow. When the annulus is very permeable, viz 1000 mD, it shows in Fig. 15 that bulk gas flow prevails in the annulus and pressure balance is readily obtainable. Under this condition, the annular pressure tends to be uniform, and the pressure at each point in the

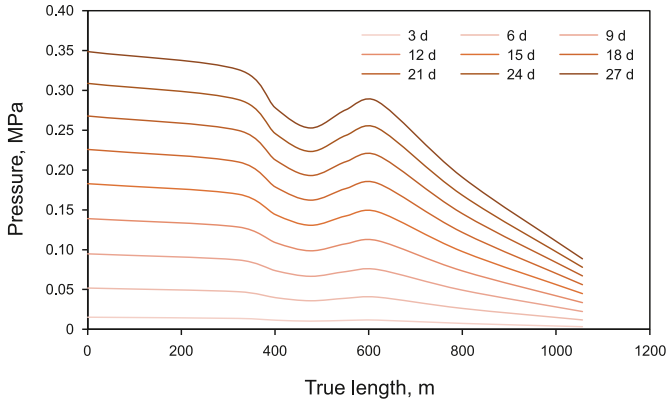

Fig. 13. Profile of pressure along the flexible pipes (gas permeability 0.1 mD).

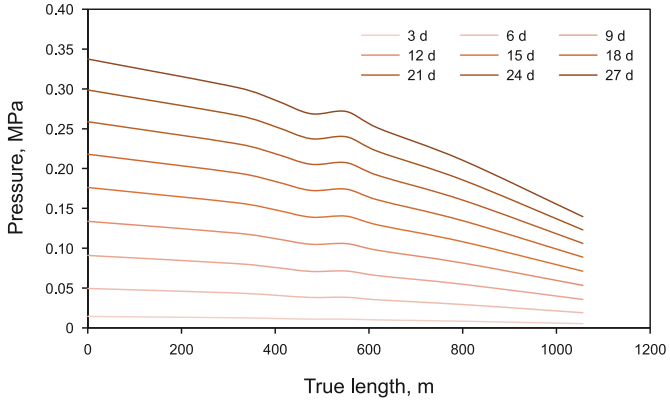

Fig. 14. Profile of pressure along the flexible pipes (gas permeability 10 mD).

annular space uniformly increases with time.

To further disclose the complex impact of annular permeability on gas transport, Figs. 16–18 present the modelled annular pressure with time at three locations, i.e., at the pipeline length of 0, 400, and 1056 m. At the onset of the pipeline where the in-pipe conditions are 3.25 MPa and 61.29 °C, Fig. 16 demonstrates that with increasing permeability more gas flows in the annulus and the pressure buildup alleviates. At 400 m where the in-pipe conditions are 2.77 MPa and 58.69 °C, Fig. 17 exhibits that the impact of annular permeability is less prominent due to both a lower in-pipe pressure and its proximity to the mid-length of the pipeline where gas flow in the annulus occurs. At the end of the pipeline, namely 1056 m in the calculation, the annual permeability exerts a profound effect on pressure because of its location at the wellhead. Fig. 18 manifests that the impact of permeability reversed at this location compared to Figs. 16 and 17. Specifically, a higher permeability enables bulk gas to flow in the annulus to the wellhead and incurs pressure buildup because of the absence of a downstream fleeing path.

4.4. Wellhead annular pressure variations

In the previous section, Fig. 18 mentioned the calculated results of annular pressure changes over time at a depth of 1056 m at the wellhead. It can be observed that the annular permeability is a significant factor influencing wellhead annular pressure. Evaluating the variation in annular pressure at the wellhead is meaningful as the annular pressure of the pipe at the wellhead is detectable. By comparing calculated values with measured values, it is possible to

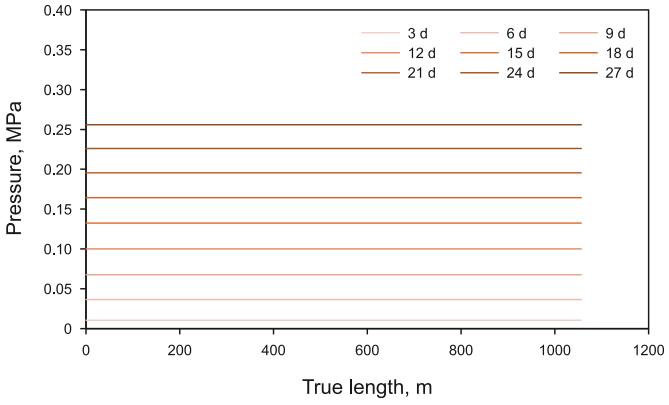

Fig. 15. Profile of pressure along the flexible pipes (gas permeability 1000 mD).

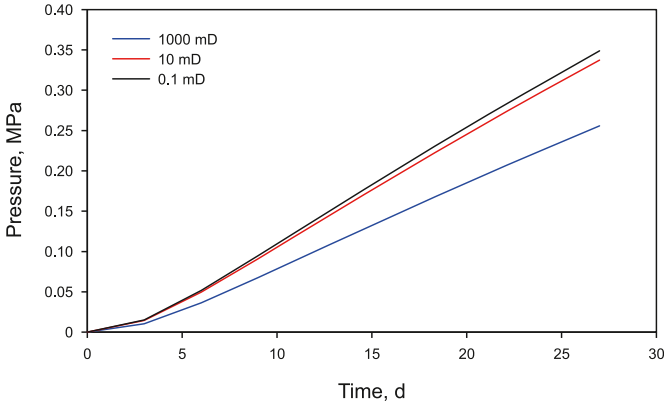

Fig. 16. Gas pressure in the annulus at 0 m under different gas permeability (3.25 MPa and 61.29 °C in bore).

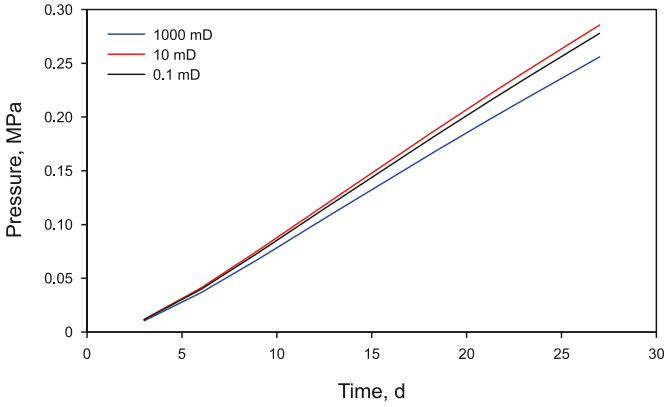

Fig. 17. Gas pressure in annulus at 400 m under different gas permeability (2.77 MPa and 58.69 °C in bore).

deduce the annular permeability.

To compare the calculated results with test data, it is essential to consider the variation in annulus control pressure during the operation of the pipe after pressure relief. Fig. 19 presents the calculated results considering annular pressure relief. On the 7th day, the annular pressure is released, and in the calculation, this is achieved by setting the annular pressure to zero. Therefore, after pressure relief, the pressure increase process is simulated directly in the calculation. It can be observed that the initial rate of pressure

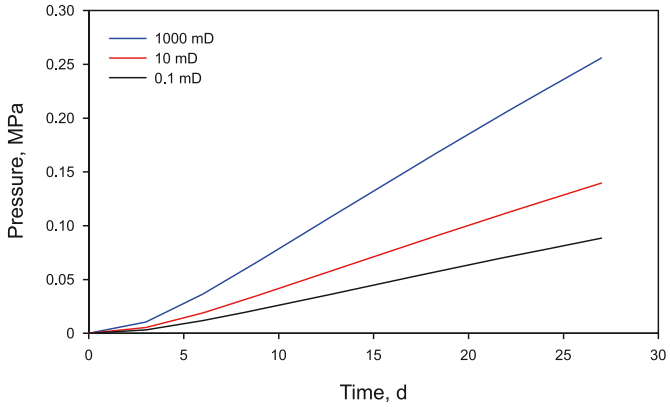

Fig. 18. Gas pressure in annulus at 1056 m under different gas permeability (1 MPa and 54.01 °C in bore).

increase is high, and the pressure increase curve becomes a convex function over time. The specific reason is that after pressure relief, although gas in the annulus can be discharged, gas continues to diffuse from the inner lining of the pipe into the annulus. The diffusion flux does not stop, and after pressure relief, as the gas concentration in the annulus rapidly decreases, the concentration gradient between the inner lining and the annulus increases. This leads to a rapid increase in the diffusion flux, reflected in the pressure curve as a swift rise.

The annular pressure test data from Well A indicates a testing period of one week. Its variation pattern aligns with the characteristic of pressure rise after pressure relief, as shown in Fig. 20. Calculations were performed to compare the pressure recovery curves after pressure relief under different permeability conditions with the test results. By adjusting the annular permeability parameters, the calculated results indicate that the test data falls between the pressure recovery curves for annular permeabilities of 123 and 512 mD.

5. Conclusion

When transporting high-pressure gas through gas transmission flexible pipes, gas molecules dissolve into the polymer lining of the flexible pipes and subsequently diffuse into the flexible pipes' annular space. The gas expansion in the annular space and the infiltration of acidic gas pose potentially adverse challenges to the structural stability of the flexible pipes. Evaluating the diffusion and permeation behavior of gas in flexible pipes through theoretical models is thus of practical significance. The main findings of this paper are as follows.

(1) The multi-layered structure of the offshore flexible pipes leads to complex gas transport phenomena. A mathematical model was developed to consider the multiphase flow inside the flexible pipes, the diffusion of gas in the inner liner, and the gas seepage in the annular space under varying permeable properties of the annulus. This modelling also included the effect of temperature on mass transport.

(2) Due to an uneven distribution of pressure and temperature in the pipeline, the multiphase flow in the pipeline underwent regime changes. With increasing gas velocity and decreasing liquid holdup, the flow regime changed from slug flow to annular flow.

(3) The diffusion of gas into the annular space is revealed to be temperature and pressure dependent. In addition, the structure and conditions of the annular space also play a role

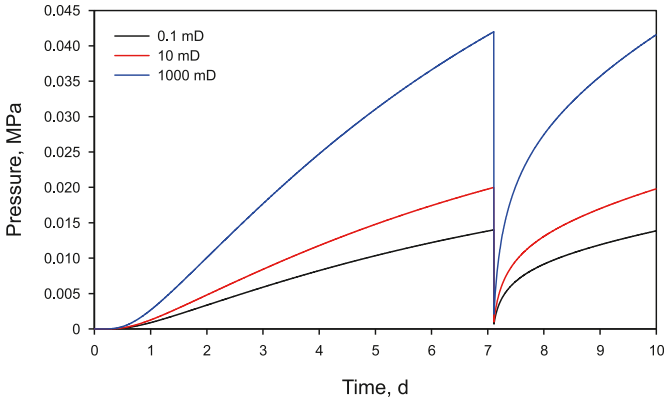

Fig. 19. Calculated results of wellhead annular pressure variations over time, taking into account the impact of pressure relief.

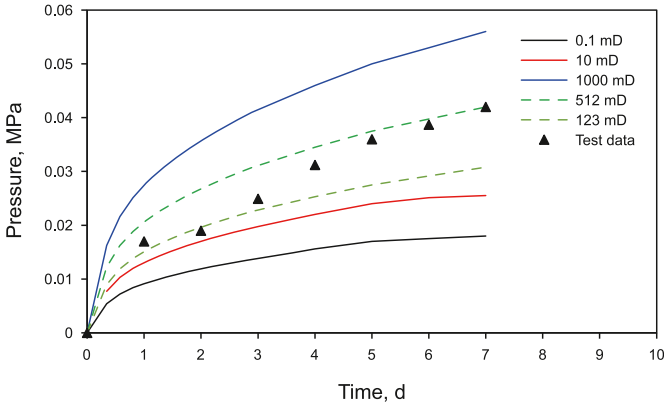

Fig. 20. Comparison of wellhead pressure recovery calculated results with test data.

in gas transport. For example, the metal layer presents a shielding effect on gas permeation.

(4) Treating the annular space as a porous medium, gas transport along the annular space was investigated. It was found that the permeability of the annual space exerts a profound impact on mass transport and, thus the distribution and site variation of pressure. In general, a higher permeability of the annulus promotes gas flow and thus helps alleviate pressure buildup. However, at the end of the pipeline, where the downstream flow path is nonexistent, a high permeability causes a substantial pressure buildup at this point.

(5) The developed mathematical model and the numerical calculation method shall also be useful in revealing the transport of condensate water and hydrates in the offshore long-distance flexible pipes.

(6) The annular permeability of the pipe affects the variation in wellhead annular pressure, with a more noticeable increase in wellhead pressure as the annular permeability increases. Typically, the wellhead annular pressure test data during actual operation is the result of pressure recovery after pressure relief, displaying a convex function pattern in the pressure increase trend. By comparing the calculated results of pressure recovery after pressure relief with the test data, a consistent pattern is observed. This supports the deduction that the annular permeability falls between 123 and 512 mD.

CRediT authorship contribution statement

Xiang-An Lu: Writing – original draft, Writing – review & editing, Conceptualization. **Liang-Liang Jiang:** Writing – review & editing, Supervision. **Jian-Sheng Zhang:** Supervision, Methodology. **Min-Gui Wang:** Writing – review & editing, Investigation.

Declaration of competing interest

The authors declare that they have no known competing financial interests or personal relationships that could have appeared to influence the work reported in this paper.

Acknowledgement

This study is supported by the Natural Science Research Project of Guangling College of Yangzhou University, China (ZKZD18004), General Program of Natural Science Research in Higher Education Institutions of Jiangsu Province, China (20KJD430006).

References

Ash, R., 2001. A note on galvanostatic time-lags. J. Membr. Sci. 5.
Ansari, A.M., Sylvester, N.D., Sarica, C., et al., 1994. A comprehensive mechanistic model for upward two-phase flow in wellbores. SPE Prod. Eng. 9 (2), 143–152.
Al-Safran, E.M., Brill, J.P., 2017. Applied Multiphase Flow in Pipes and Flow Assurance. SPE, pp. 89–122.
Barnea, D., Shoham, O., Taitel, Y., Dukler, A.E., 1985. Gas-liquid flow in inclined tubes: flow pattern transitions for upward flow. Chem. Eng. Sci. 40, 131–136. https://doi.org/10.1016/0009-2509(85)85053-3.
Chen, Y., He, M., Zong, Y., Dong, S., Yan, Y., Zhang, Y., Liu, H., Cao, J., 2021. Research progress on failure modes of unbonded flexible pipe and their control measures. Nat. Gas. Ind. 41, 122–131. https://doi.org/10.3787/j.issn.1000-0976.2021.11.013.
Emileh, A., Vasheghani-Farahani, E., Imani, M., 2007. Swelling behavior, mechanical properties and network parameters of pH- and temperature-sensitive hydrogels of poly((2-dimethyl amino) ethyl methacrylate-co-butyl methacrylate). Eur. Polym. J. 43, 1986–1995. https://doi.org/10.1016/j.eurpolymj.2007.02.002.
Flaconneche, B., Martin, J., Klopffer, M.H., 2001. Permeability, diffusion and solubility of gases in polyethylene, polyamide 11 and poly (vinylidene fluoride). Oil & Gas Science and Technology - Rev. IFP 56, 261–278. https://doi.org/10.2516/ogst:2001023.
Li, N.N., Long, R.B., 1969. Permeation through plastic films. AIChE J. 15, 73–80. https://doi.org/10.1002/aic.690150118.
Li, X., Jiang, X., Hopman, H., 2020. Predicting the wet collapse pressure for flexible risers with initial ovalization and gap: an analytical solution. Mar. Struct. 71, 102732. https://doi.org/10.1016/j.marstruc.2020.102732.
Liu, J., Ma, J., Vaz, M.A., Duan, M., 2020. Viscoelastic damping of flexible risers: theoretical model. Ocean Eng. 217, 107974. https://doi.org/10.1016/j.oceaneng.2020.107974.
Lu, X., Chen, J., Li, J., et al., 2023. Gas permeation mechanism in the annulus of flexible gas line pipes. Nat. Gas. Ind. 43 (8), 127–134. https://doi.org/10.3787/j.issn.1000-0976.2023.08.012.
Merkel, T.C., Bondar, V.I., Nagai, K., Freeman, B.D., Pinnau, I., 2000. Gas sorption, diffusion, and permeation in poly(dimethylsiloxane). J. Polym. Sci. B Polym. Phys. 38, 415–434. https://doi.org/10.1002/(SICI)1099-0488(20000201)38:3<415::AID-POLB8>3.0.CO;2-Z.
Provasi, R., Toni, F.G., de Arruda Martins, C., 2022. Friction coefficient influence in a flexible pipe: a macroelement model. Ocean Eng. 266, 112719. https://doi.org/10.1016/j.oceaneng.2022.112719.
Ren, S., Tang, W., Kang, Z., Geng, H., 2020. Numerical study on the axial-torsional response of an unbonded flexible riser with damaged tensile armor wires. Appl. Ocean Res. 97, 102045. https://doi.org/10.1016/j.apor.2019.102045.
Rutherford, S.W., Do, D.D., 1997. Review of time lag permeation technique as a method for characterisation of porous media and membranes. Adsorption 3, 283–312. https://doi.org/10.1007/BF01653631.
Sadrzadeh, M., Amirilargani, M., Shahidi, K., Mohammadi, T., 2011. Pure and mixed gas permeation through a composite polydimethylsiloxane membrane. Polym. Adv. Technol. 22, 586–597. https://doi.org/10.1002/pat.1551.
Shoham, O., 2006. Mechanistic Modeling of Gas-Liquid Two-phase Flow in Pipes. SPE, TX.
Scheichl, R., Klopffer, M., Benjelloundabaghi, Z., Flaconneche, B., 2005. Permeation of gases in polymers: parameter identification and nonlinear regression analysis. J. Membr. Sci. 254, 275–293. https://doi.org/10.1016/j.memsci.2005.01.019.
Taitel, Y., Barnea, D., Dukler, A.E., 1980. Modelling flow pattern transition for steady upward gas-liquid flow in vertical tubes. AIChE J. 26 (3), 345–354.

Vantadori, S., Carpinteri, A., Iturrioz, I., 2019. Fretting failure of a pressure armour in an unbonded flexible riser. Int. J. Fatig. 128, 105203. https://doi.org/10.1016/j.ijfatigue.2019.105203.
Wang, K., Yu, X., Zheng, L., Zhang, E., He, Y., 2021. Numerical investigation of gas permeation and condensation behavior of flexible risers. J. Petrol. Sci. Eng. 203, 108622. https://doi.org/10.1016/j.petrol.2021.108622.
Wang, K., Zhang, J.J., Yu, B., Zhou, J., Qian, J.H., Qiu, D.P., 2009. Numerical simulation on the thermal and hydraulic behaviors of batch pipelining crude oils with different inlet temperatures. Oil & Gas Science and Technology - Rev. IFP 64, 503–520. https://doi.org/10.2516/ogst/2009015.
Wu, B., Firouzi, M., Mitchell, T., Rufford, T.E., Leonardi, C., Towler, B., 2017. A critical review of flow maps for gas-liquid flows in vertical pipes and annuli. Chem. Eng. J. 326, 350–377. https://doi.org/10.1016/j.cej.2017.05.135.